Materials Letters 277 (2020) 128177

Contents lists available at ScienceDirect

Materials Letters

journal homepage: www.elsevier.com/locate/mlblue

Low cost flexible ultraviolet photodetector based on ZnO nanorods prepared using chemical bath deposition

Salah M. Saleh Al-Khazali [a,b], Husam S. Al-Salman [a], A. Hmood [a,*]

[a] Microelectronics and Nanotechnology Research Laboratory (M. N. R. Lab.), Physics Dept., College of Science, Basrah University, Basrah, Iraq
[b] The General in Directorate of Education in Al-Najaf Al-Ashraf, Ministry of Education-Najaf, Iraq

ARTICLE INFO

Article history:
Received 21 May 2020
Received in revised form 12 June 2020
Accepted 16 June 2020
Available online 21 June 2020

Keywords:
Flexible Substrate
CBD method
ZnO NRs
UV photodetector

ABSTRACT

This report involves a novel fabrication of ultraviolet (UV) photodetector (PD) based on ZnO nanorods (NRs) onto flexible polypropylene carbonate (PPC) substrate, ZnO/PPC, using chemical bath deposition (CBD). The structural, morphological and optical properties of the samples were studied by utilizing X-ray diffraction (XRD), field emission scanning electron microscopy (FESEM), energy dispersive X-ray spectra (EDX), and UV–Vis spectrophotometer. The photosensitivity values of the ZnO/PPC PD were determined to be 52.48, 47.46, and 42.53 toward wavelength of 385 nm at bias voltage of 5, 10 and 15 V, respectively. The response and the recovery times were good value when ZnO/PPC (PD) illuminated under ON/OFF UV pulse of 375, 385 and 405 nm at 5, 10, and 15 V bias voltages. The maximum values of the current gain and the quantum efficiency (η), are 1.52 and 550.7 under UV illumination of 385 nm at 5 V and 15 V, respectively.

1. Introduction

Over the decades, the rapid increases within the number of discoveries of flexible Zinc Oxide nanorods (*ZnO NRs*) photodetector (*PD*) have been observed. The Flexible electronic devices has been received a good attention due to the likelihood to use it as low-cost sensors operating at ultraviolet (*UV*) wavelength with narrow band response detection [1]. *UV* photodetection is essential feature for numerous applications; for instance, water purification system, flame monitor, money counting, and photochemical phenomena revelation [2]. Due to unique properties such as a wide bandgap (E_g) of 3.37 eV, high exciton binding energy (60 meV), low cost, and simple manufacture, the ZnO nanostructure consider a promising material as potential candidate for optoelectronic applications [3]. Flexible polypropylene carbonate (*PPC*) substrate was chosen since it has lightweight, low chemical reactivity, high surface resistivity and high dielectric resistance over large frequencies which motivated the scientists to use it in various applications [4]. Several deposition techniques have been reported to deposit ZnO nanostructures including radio frequency (*RF*) sputtering [5], pulsed laser deposition (*PLD*) [6], and chemical bath deposition (*CBD*) [7]. In the present paper, the first *CBD* preparation of ZnO *NRs* onto *PPC* substrate is presented. In this study, the ZnO *NRs* onto *PPC* substrate using *CBD* route for UV detection application has been demonstrated.

2. Experimental part

ZnO *NRs* were fabricated onto the *PPC* substrate using the *CBD* technique. *PPC* substrate was ultrasonically cleaned using ethanol, acetone, and deionized water (5 min duration time for each) followed by deposit a ZnO seed layer through the Spin-Coating technique. Zinc acetate dehydrate [$Zn(CH3COOH)_2{\cdot}2H_2O$], 0.1 M, was dissolved in ethanol and poured over the center of a PPC substrate at a rate of 3000 rpm for 35 s, then dried at 150 °C for 5 min. This process was repeated for six times. Finally, the sample was annealed at 180 °C for 1 h. The ZnO/PPC seed layer was fixed vertically in container contain a preheated solution, 95 °C, of equimolar concentration of Zinc nitrate hexahydrate ($Zn(NO_3).6H_2O$) and hexamethylenetetramine ($C_6H_{12}N_4$), in deionized water for 2 h. A flexible metal–semiconductor–metal (*MSM*) *UV PD* was fabricated by depositing electrodes of aluminum (*Al*) on top of ZnO *NRs* film through a metal mask using thermal evaporation technique (Fig. 1). In this work, the *XRD* measurement and *FESEM* images with *EDX* analysis were performed using SIEMENS D500 and ZEISS SUPER 55VP equipped with an *EDX* system, respectively. The optical properties were investigated using Shimadzu-1650 UV–Vis spectrometer. Current-voltage (*I-V*) and photoresponse properties were measured by Keithley-2430 source meter and Fluke-8808

* Corresponding author.
E-mail address: arshad.phy73@gmail.com (A. Hmood).

https://doi.org/10.1016/j.matlet.2020.128177
0167-577X/

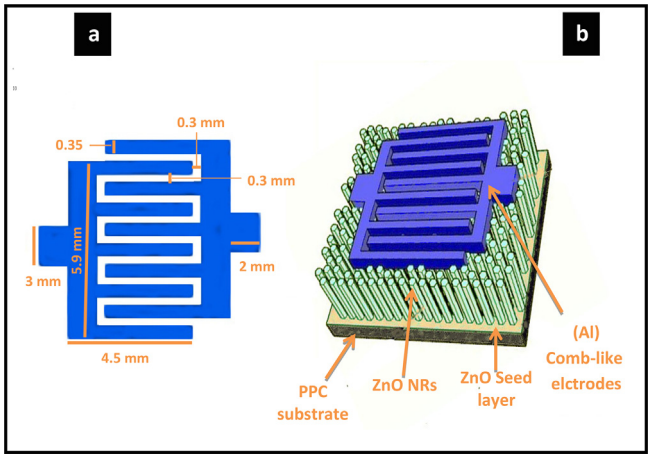

Fig. 1. Schematic of: (a) Al comb-like electrodes, and (b) the design of the ZnO/PPC photodetector.

DMM respectively, connected to PC for data analysis using *UV* wavelengths of 375, 385 and 405 nm illumination.

3. Results and discussion

3.1. Crystal structure analysis

The *XRD* pattern and Surface morphology images of the ZnO/PPC *NRs* film were shown in Fig. 2. The *XRD* spectrum (Fig. 2a) reveals a hexagonal wurtzite structure with the preferred orientation belong (002) phase at 34.44° corresponds to *JCPDS* card No. 36–1451 [8,9]. The crystalline size unit and *FWHM* were 70.53 nm and 0.118 which revealed a good quality of ZnO *NRs*.

3.2. Surface morphology

The *FESEM* images (Fig. 2b) illustrate that the ZnO *NRs* array have a uniform distribution with interstitial space, homogenous, hexagonal (inset of Fig. 2b), and vertically aligned on the *PPC* substrate with an average diameter of 90 to 130 nm as shown in Fig. 2 (c). The *NRs* length of 1.96μm were estimated from the cross-section image illustrate in Fig. 2(d). Fig. 2(e) shows the *EDX* spectrum peaks which identifies as zinc, oxygen, and carbon. The presence of carbon results from *PPC* substrate.

3.3. Optical properties

The absorption and transmission spectra of ZnO *NRs* film are shown in Fig. 3(a). The absorption spectrum of the film reveals the high and sharp absorbance value in the wavelength range of 300–385 nm in the *UV* region and high optical transmission value within the visible region of the spectrum. The fundamental absorption for ZnO *NRs* film may be due to the allowed direct transitions described by the well-known relation as follows:

$$\alpha h\upsilon = A_{\alpha}(h\upsilon - Eg)^{1/2} \quad (1)$$

where α is the absorption coefficient, $h\upsilon$ is the incident photon energy, E_g is the energy bandgap, and A_α is the characteristic parameter independent of the photon energy for respective transitions [7]. The E_g value of 3.177 eV was estimated by plotting $(\alpha h\upsilon)^2$ vs $h\upsilon$ as shown in Fig. 3(b). This value agreed well with the results reported previously [6,10,11].

3.4. Photodetector characteristics

Fig. 3(c) depicts the *I–V* curves of ZnO/PPC *PD* in the dark and under *UV* wavelength of 385 nm (40 μW/cm^2) with ohmic behavior indicating good contact between the ZnO *NRs* and the Al electrodes. The dark current (I_{dark}) and photocurrent (I_{ph}) values were 9.67 μA and 26.49 μA respectively, with current gain (I_{ph}/I_{dark}) of 2.7. To investigate the effect of bias voltage on the I_{ph} behavior of ZnO/PPC *PD*, the I_{ph} as a function of interval time $(I-t)$ at various voltages under the turned ON/OFF *UV* light illumination of 385 nm was depicted in Fig. 3(d). It's obvious that increments of the photocurrent value with increasing bias voltage cause to increase of carriers drift velocity v, that is directly dependent on the applied bias voltage V (as in equation $v = \mu V/1$ where μ represents the carrier's mobility and lis the separation between the electrodes) and the decrease in the carrier's transit time T_t (e.g.$T_t = 1^2/\mu v$) [12]. The I_{dark} and I_{ph} level remain stable without deviation even after many cycles. Fig. 3(e), (f) and (g) shows the $(I-t)$ curve at 5 V, 10 V, and 15 V bias voltage respectively, under the turned ON/OFF various UV light illuminations (375 nm, 50 μW/cm^2; 385 nm, 40 μW/cm^2; 405 nm, 0.45 mW/cm^2). It can be observed that after several cycles, the maximum photocurrent value is almost steady at all bias voltages, which indicates that the flexible *PD* has good stability and high reproducibility. The photosensitivity (S_{ph}) has been calculated using the relation [13]:

$$S_{ph}(\%) = \left(\frac{I_{ph} - I_{dark}}{I_{dark}}\right) \times 100 \quad (2)$$

Quantum efficiency η of the *PD* can be realized employing the following relation [3]:

$$\eta(\%) = \left[\frac{I_{ph}}{q}\frac{h\upsilon}{P_{in}}\right] \times 100 \quad (3)$$

where P_{in}, h, q and v are incident power, Plank constant, electric charge, and the frequency of incident light, respectively. Based on Fig. 3(d-g) and Eqs. (2) and (3), the I_{ph}, I_{dark}, S_{ph}, and η were calculated and listed in Table 1. The photosensitivity S_{ph} value of the ZnO/PPC *PD* under UV light of 385 nm were 52.48, 47.46, and 42.53 at 5, 10, and 15 V bias voltage respectively, which is higher that obtained from 375 nm and 405 nm. However, increase the bias voltage to 10 V and 15 V lead to decrease S_{ph} values for all *UV* wavelengths. Based on $(I-t)$ characteristics, the *PD* has maximum current gain of 1.52 under *UV* light of 385 nm and 5 V bias voltage. The quantum efficiency (η), Table 1, increases with increasing the bias voltage and reach its maximum value of 550.7 under *UV* illumination of 385 nm at 15 V. This maximum value results because of the high photocurrent at 15 V compare with those at 5 and 10 V. The response time τ_{Res} (is the required time for the current to reach 90% of the maximum value of I_{ph}) and the recovery time τ_{Rec} (is the required time for the current to decay to 10% of the maximum I_{ph}) were calculated based on Fig. 3(e-g). The *PD* exhibit τ of 66.4, 33.09 and 93.2 ms and τ_{Rec} of 97, 83.4 and 126 ms (Table 1) at 5, 10 and 15 V respectively, under *UV* light of 405 nm. This results were better than those reported previously [1,8,10]. In addition, Table 1 reveals the fast response and recovery times under *UV* light of 405 nm compare with 375 and 385 nm. In General, the recovery time relatively longer than response time which might be caused by the slow relaxation time of carrier in the deep defect states compared with that of the surface state process [14–16] besides the interspaces that exist between the ZnO *NRs*. The photosensitivity results and $(I-t)$ curve demonstrated good photodetection characteristics and high reproducibility.

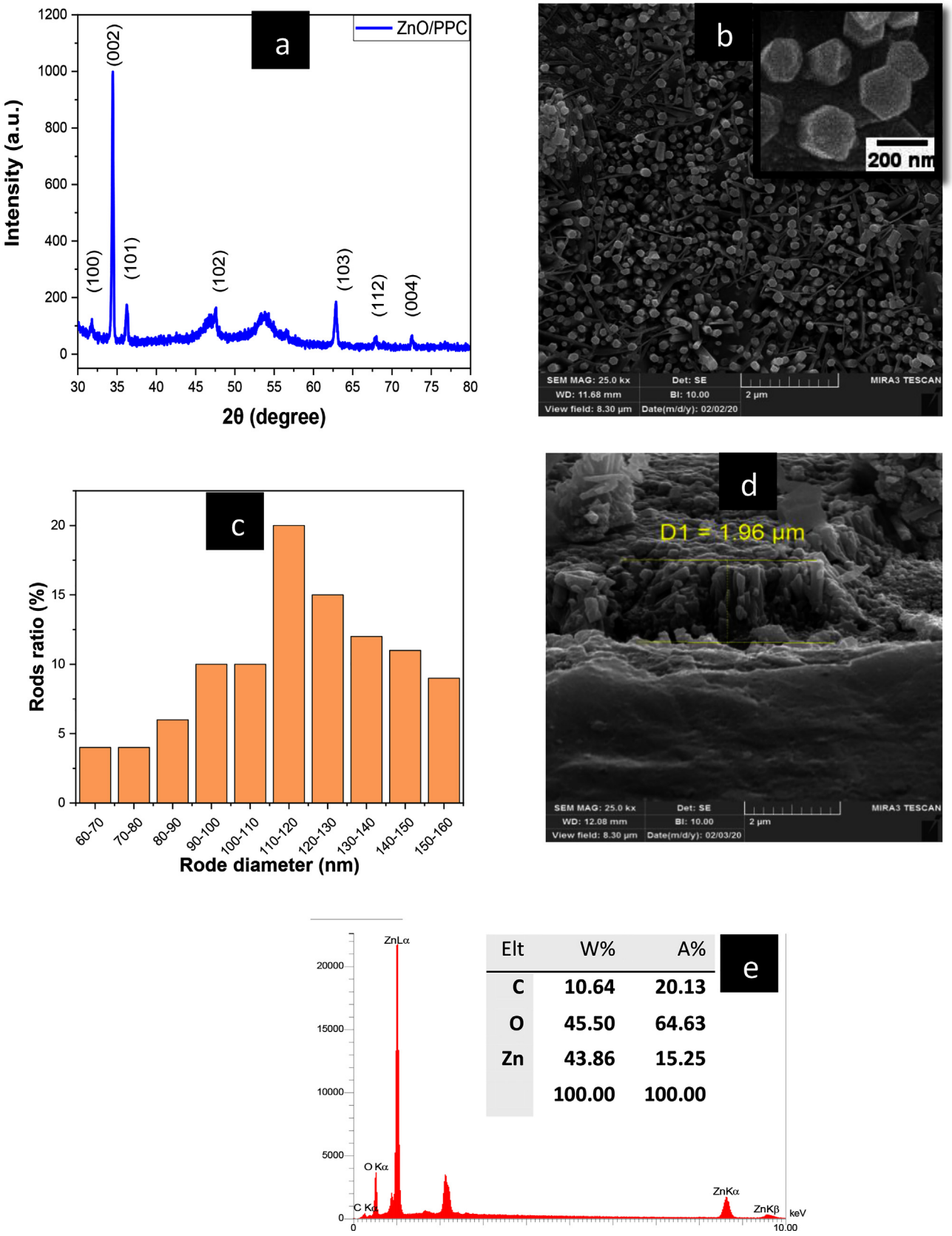

Elt	W%	A%
C	10.64	20.13
O	45.50	64.63
Zn	43.86	15.25
	100.00	100.00

Fig. 2. The structural and surface morphology of the ZnO/PPC sample: (a) XRD patterns, (b) FESEM image, (c) Histogram distribution of the NR diameters, (d) Cross-session, and (e) EDX spectrum.

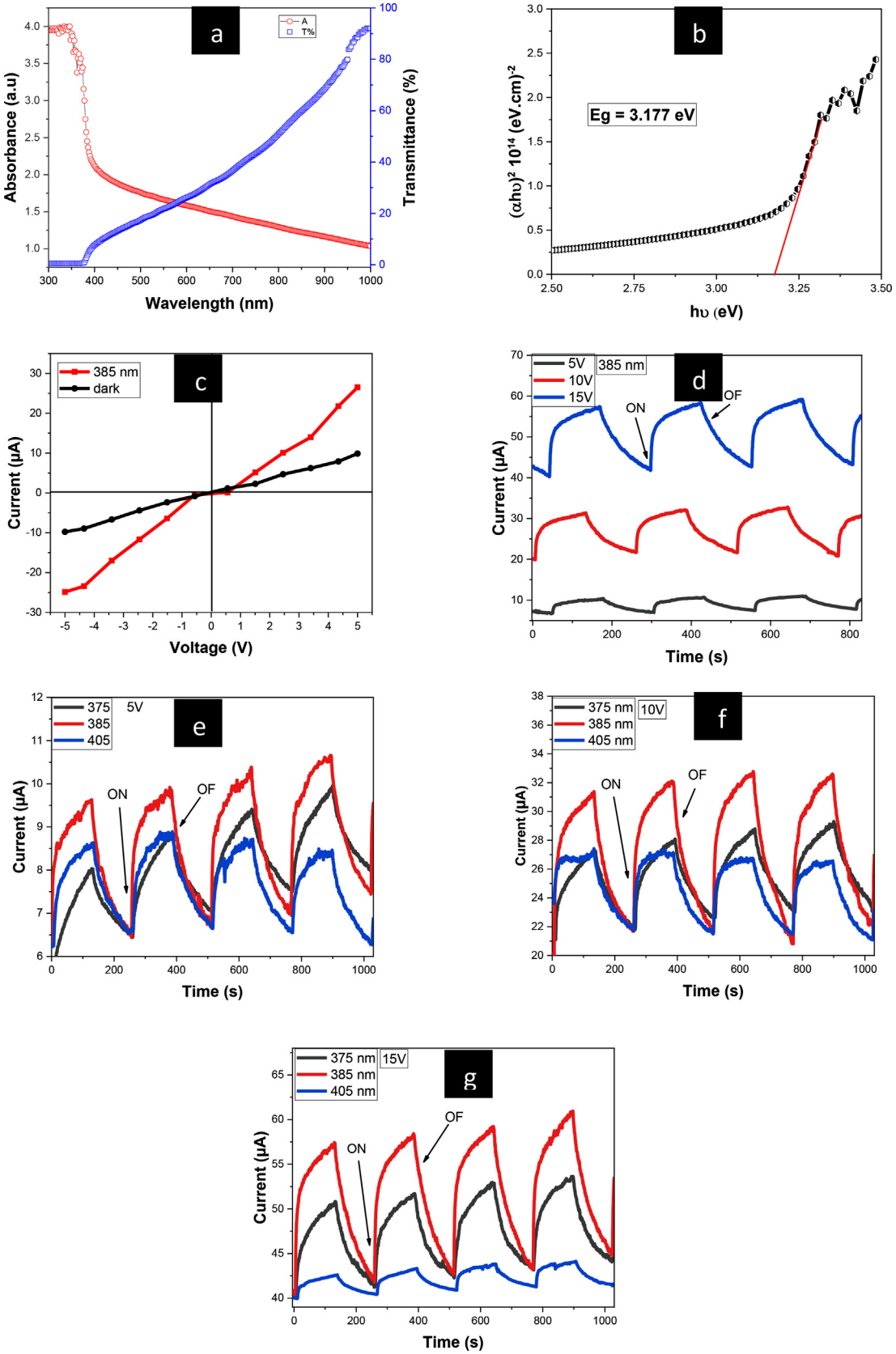

Fig. 3. The optical and electrical properties of the ZnO/PPC photodetector: (a) The absorbance and transmittance spectrum, (b) Plot of $(\alpha h\nu)^2$ vs. $h\nu$, (c) I–V characteristics in the dark and under UV illumination of 375, 385, and 405 nm wavelength, (d) Photocurrent response spectra toward 385 nm wavelength at various bias voltage; and (e), (f), and (g) Photocurrent response spectra toward 375, 385 and 405 nm wavelengths at 5 V, 10 V, and 15 V respectively.

Table 1
The photoresponse prameters of ZnO/PPC photodetector exposure to various UV wavelengths.

Bias voltage (V)	Wavelength (nm)	τ_{res}(ms)	τ_{rec}(ms)	$I_{dark}(\mu A)$	$I_{ph}(\mu A)$	Current gain	S_{ph}(%)	η(%)
5	375	98	130.5	6.44	8.82	1.36	36.95	62.95
	385	69.5	109.3	6.44	9.82	1.52	52.48	108.8
	405	66.4	97	6.62	8.83	1.33	33.38	6.014
10	375	85.39	115.1	21.8	28.0	1.28	28.44	164.0
	385	63.64	93.4	21.7	32.0	1.47	47.46	331.7
	405	33.09	83.4	21.7	27.1	1.24	24.88	14.69
15	375	95.97	115.8	40.2	50.7	1.26	26.11	277.7
	385	71.81	120.3	40.2	57.3	1.42	42.53	550.7
	405	93.2	126	39.9	42.5	1.06	6.51	7.075

4. Conclusion

The flexible photodetector based on ZnO *NRs* was successfully fabricated onto *PPC* substrate using *CBD* method. The results showed high stability over time, good sensitivity (52.48%), quantum efficiency (108.8%), and a high photocurrent upon exposure to 385 nm, the response time (66.4 s), and recovery time (97 s) upon exposure to 405 nm when applying a bias voltage of 5 V. The high photocurrent and photosensitivity of the *PD* could be attributed to the high surface-to-volume ratio in addition to good crystal structure. The results indicate a promising flexible high performance photodetector.

CRediT authorship contribution statement

Salah M. Saleh Al-Khazali: Conceptualization, Methodology, Writing - review & editing, Supervision. **Husam S. Al-Salman:** Investigation, Supervision, Writing - review & editing. **A. Hmood:** Writing - original draft, Writing - review & editing.

Declaration of Competing Interest

The authors declare that they have no known competing financial interests or personal relationships that could have appeared to influence the work reported in this paper.

Acknowledgements

The authors gratefully acknowledge support from department of Physics, College of Science, University of Basrah, Iraq.

References

[1] I.C. Yao, T.Y. Tseng, P. Lin, Sensor Actuat A-Phys. 178 (2012) 26–31.
[2] K.W. Liu, J.G. Ma, J.Y. Zhang, Y.M. Lu, D.Y. Jiang, B.H. Li, D.Z. Shen, Solid State Electron. 51 (2007) 757–761.
[3] H.S. Al-Salman, M.J. Abdullah, J. Mater. Sci. Technol. 29 (2013) 1139–1145.
[4] N.N. Jandow, F.K. Yam, S.M. Thahab, H.A. Hassan, K. Ibrahim, Curr. Appl. Phys. 10 (2010) 1452–1455.
[5] S.I. Inamdar, K.Y. Rajpure, J. Alloy. Comp. 595 (2014) 55–59.
[6] S.H. Ribut, C.A.C. Abdullah, M.Z.M. Yusoff, Results Phys. 13 (2019) 102146.
[7] H.S. Al-Salman, M.J. Abdullah, Sensors Actuators B: Chem. 181 (2013) 259–266.
[8] Y.L. Chu, L.W. Ji, H.Y. Lu, S.J. Young, I.T. Tang, T.T. Chu, Y.T. Tsai, J. The Electrochem. Soc. 167 (2020) 027522.
[9] Q. Xie, X. Liu, H. Liu, Superlattices Microstruct. (2020) 106391.
[10] K.C. Verma, N. Goyal, R.K. Kotnala, Phys. Chem. Chem. Phys. 21 (2019) 12540–12554.
[11] N.N. Jandow, H.A. Hassan, F.K. Yam, K. Ibrahim, Photodetectors. (2012) 1–32.
[12] M.S. Mahdi, N.M. Ahmed, A. Hmood, K. Ibrahim, M. Bououdina, Mate. Sci. Semi. Proc 100 (2019) 270–274.
[13] F.H. Alsultany, Z. Hassan, N.M. Ahmed, Optical Mater. 60 (2016) 30–37.
[14] J. Sun, F.J. Liu, H.Q. Huang, J.W. Zhao, Z.F. Hu, X.Q. Zhang, Y.S. Wang, Appl. Surface Sci. 257 (2010) 921–924.
[15] S.M.A. Rastialhosseini, A. Khayatian, R. Shariatzadeh, M.A. Kashi, Appl. A-Phys. 125 (2019) 829.
[16] Y. Xie, L. Wei, G. Wei, Q. Li, D. Wang, Y. Chen, S. Yan, G. Liu, L. Mei, J. Jiao, Nanoscale Res. Lett. 8 (2013) 1–6.